

Reactive energy in non-diffracting localized waves

Peeter Saari^{1,2*} and Ioannis Besieris³

¹*Institute of Physics, University of Tartu, W. Ostwaldi 1, 50411, Tartu, Estonia*

²*Estonian Academy of Sciences, Kohtu 6, 10130 Tallinn, Estonia and*

³*The Bradley Department of Electrical and Computer Engineering,
Virginia Polytechnic Institute and State University, Blacksburg, Virginia 24060, USA*

(Dated: November 5, 2019)

It is well known that although the group velocity of structured light pulses propagating in vacuum can be subluminal or superluminal, the upper limit of the energy flow velocity is c , the speed of light in vacuum. This inequality can be explained in terms of the reactive energy left behind by the fields. Energy and reactive energy densities have been calculated for vector-valued two-dimensional (light sheet) superluminal electromagnetic nondiffractive pulses, as well as scalar-valued and TM three-dimensional superluminal and subluminal spatiotemporally localized electromagnetic waves. Emphasis is placed on the physical formation of the reactive energy due to interference of the plane-wave constituents of the structured light waves.

PACS numbers: 42.25.Bs, 42.25.Fx, 42.60.Jf, 42.65.Re

I. INTRODUCTION

It is well known that in the case of electromagnetic (EM) one-dimensional plane wave pulses in vacuum, not only the phase velocity but also the group and energy flow velocities are equal to the universal constant c . But it is not so when the wave is spatially confined, i.e., generally in the case of structured light. For example, in a pulsed Gaussian beam, the group velocity v_g may not be only luminal ($v_g/c = 1$), but also slightly superluminal ($v_g/c > 1$) or subluminal ($v_g/c < 1$) locally in the beam waist region. Which alternative takes place depends on how the frequency and the waist width of every monochromatic Gaussian beam constituent of the pulsed beam are coupled with each other. Subtleties of relations between the pulse group velocity and the measurable travel time, as well as some relevant contradictions in the recent literature, are analyzed in Ref. [1].

A wide class of structured light pulses, called non-diffracting localized waves, is characterized by a specific type of space-time coupling. For all monochromatic plane-wave constituents of such pulsed waves, there is a linear functional dependence between their temporal frequency ω and the component k_z of the wave vector, which lies in the direction of propagation of the pulses, rendering the latter propagation-invariant. This means that the spatial distribution of the pulse energy density does not change in the course of propagation—it does not spread either in the lateral or in the longitudinal direction (or temporally). In reality, such a non-diffracting (non-spreading) propagation occurs over a large but still finite distance, because the aforementioned frequency-wavenumber functional dependence is not strict for practically realizable (finite-energy and finite aperture) pulses.

The first versions of propagation-invariant localized pulsed waves were theoretically discovered in the late 1980-ies, and since then a massive literature has been devoted to them. (See collective monographs [2, 3] and reviews [4–9]). The realizability of them in optics was first demonstrated in Ref. [10] for the so-called Bessel-X pulse which is the only propagation-invariant pulsed version of the monochromatic Bessel beam introduced in Ref. [11]. The group velocity of Bessel-X pulses exceeds c , i.e., it is superluminal in empty space without the presence of any resonant medium. This strange property has been widely discussed in the literature referred to above and was experimentally verified by several groups [12–15] for cylindrically symmetric 3D pulses. For 2D (light sheet) counterparts of such propagation-invariant pulses measurements of various group velocities have been recently carried out by Abouraddy’s group at the University of Central Florida [16–18].

In our recent paper [19], the following question was dealt with: how is the group velocity of propagation-invariant pulses related—if it is related at all—to the energy flow velocity in them? Definitely, the statement “if an energy density is associated with the magnitude of the wave ... the transport of energy occurs with the group velocity, since that is the rate of which the pulse travels along” (citation from Ref. [20], section 7.8) cannot hold if the group velocity exceeds c . For, no electromagnetic field can transport energy faster than c even in the case of superluminal pulses [21–23] (see also Ref. [19]).

Indeed, it is shown in Ref. [19] that the velocity v_e , with which energy in non-diffracting pulsed EM and scalar waves locally flows in the direction of propagation, is not equal to the propagation velocity (group velocity v_g) of the pulse itself, but these two quantities obey the simple relation

$$\frac{v_e}{c} = \frac{2\beta}{1 + \beta^2}, \quad (1)$$

where $\beta = v_g/c$. Here, we summarize the properties of

* Corresponding author: peeter.saari@ut.ee

this physically content-rich relation in Fig. 1. We see that regardless of whether the pulse propagates subluminally ($\beta < 1$) or superluminally ($\beta > 1$), the energy flow velocity v_e does not exceed c . But it is surprising that the value of v_e is the same for both a subluminal and a superluminal pulse: this is seen from the mirror symmetry of the curve v_e/c with respect to the vertical line at $v_g/c = 1$ of the log-log plot in Fig. 1 and results from the invariance of Eq. (1) with respect to the replacement $\beta \rightarrow 1/\beta$.

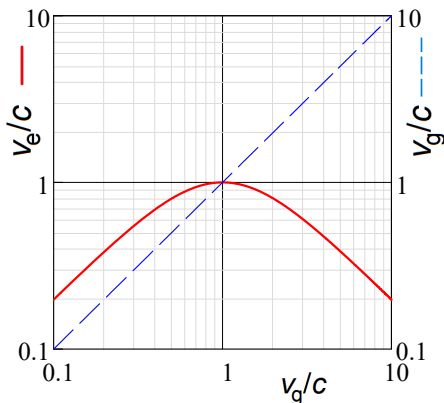


FIG. 1. Plot of Eq. (1) in decimal logarithmic scales. The curve of the energy flow velocity is juxtaposed to the straight line of unit slope, which would represent the energy flow velocity versus the group velocity if they were equal.

It follows from Fig. 1 that in the case of a superluminal pulse energy propagates slower than the pulse itself and in the case of a subluminal pulse energy propagates faster than the pulse itself. Such counterintuitive situations as if energy is lagging behind a superluminal pulse, or as if outrunning a subluminal pulse, are explained in Ref. [19] by the presence of the reactive energy in nondiffracting fields.

Reactive energy near sources of electromagnetic fields and in free standing waves was thoroughly studied by Kaiser [24], who also proposed to use the term 'energy flow velocity' for distinction from the time-independent 'energy transport velocity' which involves only averages over one period in the time-harmonic case. He also introduced the term 'electromagnetic inertia density' defined as the reactive energy density divided by c^2 . Reactive energy appears everywhere where there is an interference between plane wave constituents in the free field. Such reactive energy is inherent to structured light fields and can be interpreted as non-zero mass of photons [25–29]. Kaiser's electromagnetic inertia density is in other words the density of mass of a classical EM field, which is a Lorentz-invariant quantity [27, 28].

The aim of the present paper is to study the formation and spatiotemporal distribution of the reactive energy in typical nondiffracting pulses. We hope that such study will enable better understanding of the counterintuitive difference between velocities of pulse propagation and en-

ergy flow.

The paper has been organized as follows. In Section II we derive an expression for the reactive energy density of a single-cycle propagation-invariant transverse magnetic (TM) two-dimensional (2D) superluminal field. We start with the 2D case, i.e., with a light sheet, not only for the simplicity of such a model but also having in mind that pulsed light sheets have practical value, e.g., in microscopy, and are presently studied intensively [16, 30–32]. Section III deals with the reactive energy density of the X wave—the scalar-valued version of which is the most studied superluminal localized wave. In Section IV we consider the reactive energy density in some simple subluminal propagation-invariant pulses. Finally, we discuss the results and, in particular, the formation and Lorentz invariance of the reactive energy density—or, equivalently, of the invariant mass density—in structured light fields. Appendices A and B consider the Lorentz invariance of the reactive energy density for vector-valued and scalar electromagnetic fields, respectively. The third Appendix describes the derivation of TM fields from scalar ones.

II. REACTIVE ENERGY IN A SINGLE-CYCLE SUPERLUMINAL LIGHT SHEET

We start with fields that do not depend on one lateral, say y , coordinate. Although such 2D fields are simpler, their properties, relevant for our study, are the same as those of cylindrical 3D ones.

Consider a TEM pulsed 2D wave propagating along the positive z direction in vacuum,

$$\mathbf{E}(x, z, t) = U(z-ct)\mathbf{e}_x, \quad \mathbf{B}(x, z, t) = c^{-1}U(z-ct)\mathbf{e}_y, \quad (2)$$

where SI units are assumed, with $\varepsilon_0\mu_0 = 1/c^2$, and \mathbf{e}_x and \mathbf{e}_y are unit vectors of a right-handed rectangular coordinate system. U is generally an arbitrary real localized function of *one* argument.

The energy flux density (Poynting vector) and the energy density of the field are generally expressed in SI units by

$$\mathbf{S} = c^2\varepsilon_0 \mathbf{E} \times \mathbf{B}, \quad (3)$$

$$w = \frac{1}{2}\varepsilon_0\mathbf{E}^2 + \frac{1}{2}\varepsilon_0c^2\mathbf{B}^2. \quad (4)$$

For the given simple field the expressions reduce to $\mathbf{S} = c\varepsilon_0U^2(z-ct)\mathbf{e}_z$ and $w = \varepsilon_0U^2(z-ct)$, respectively.

Following Refs. [24, 27], the reactive (rest) energy density is defined as

$$R = \sqrt{w^2 - \mathbf{S}^2/c^2}, \quad (5)$$

which by using Eqs. (2), (3), and (4) turns to zero in the given case. Thus, a plane wave pulse does not possess reactive energy and, accordingly, the energy flow velocity is c —well-known results.

Let us take now a symmetrical pair of plane waves—the propagating direction of the first one lies on the (x, z) plane and is inclined by angle $+\theta$ with respect to the z -axis, and the second one by angle $-\theta$ on the same plane. In this case, the coordinate z in Eq. (2) is replaced by $z \cos \theta + / - x \sin \theta$ for a member of the pair, respectively. The components of the vectors \mathbf{E} and \mathbf{B} for both waves transform also according to the rules of rotation around the axis y . For the polarizations given in Eq. (2), the magnetic field remains polarized along the y axis. However, the electric field has both x and z components. Thus, we are dealing with a transverse magnetic (TM) field. The resulting expressions for \mathbf{S} , w , and R are rather cumbersome and omitted here; for \mathbf{S} and w at points along z axis they are given in Ref. [19].

Instead, we have evaluated Eq. (5) numerically, specifying the function U —for clarity of the following interpretation—as an optical single-cycle pulse of the form $U(\zeta) = A \sin \zeta$, if $|\zeta| \leq \pi$, $U(\zeta) = 0$, if $|\zeta| > \pi$, where A is an amplitude constant with dimension [V/m], which is equated to unity. The results are presented in Fig. 2.

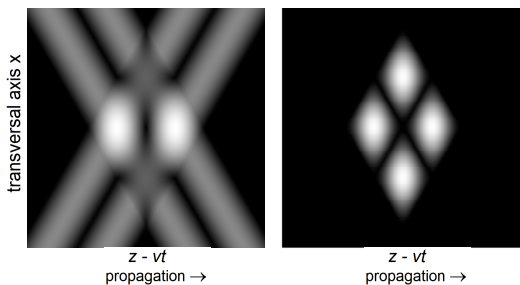


FIG. 2. Greyscale plots of the energy and reactive energy densities of the field of two single-cycle TM plane-wave pulses propagating under angles 30° and -30° , respectively, with respect to the z axis. Depicted is the interference region as a propagation-invariant superluminal 2D pulse moves along the z axis with velocity $v = c/\cos 30^\circ = 1.15c$. Left plot: energy density from Eq. (4) (for lower contrast of the greyscale, \sqrt{w} has been plotted). Right plot: reactive energy density according to Eq. (5). Axes $z - vt$ and x have the same range $(6\lambda/5)[-1, 1]$, where λ is the wavelength of the single-cycle component pulse (which is equal to the length of the whole pulse). The ratio of the maximum values of the energy and reactive energy densities is $\max(w)/\max(R) = 7$.

The propagation invariance of the X-like pattern in the course of propagating along the z axis manifests itself as a dependence on the combined variable $z - vt = z - (c/\cos \theta)t$, or on its rescaled version $z \cos \theta - ct$ (from here on we omit the subscript g denoting the group velocity for brevity $v \equiv v_g$). The plots can be taken as “snapshots in flight”, i.e., spatial distributions of the densities at a fixed time instant (say, $t = 0$), or, as temporal dependence along the transversal axis x at a fixed value of the coordinate z (say, $z = 0$). For clarity, below we will use the former interpretation. Of course, we could say that the plots show purely the spatial dependence in

terms of the “co-propagating” variable $\zeta = z - vt$ and the variable x . However, such an interpretation would imply a Galilean transformation into an unphysical superluminally moving frame, which should not be confused with the Lorentzian transformation considered below. The energy density at the two interference maxima is 3.5 times higher than outside of the interference region (where it has taken to be equal to one). The ratio would be equal to 4 if the electric field vectors of the two pulses were parallel as the magnetic field vectors do. For the same reason, the energy density in the two regions of destructive interference of the magnetic fields is not zero, but has a value equal to 0.5. Understandably these ratios depend on the value of the angle θ as will be reasoned below. Let us notice that defining the model single-cycle pulse with abrupt beginning and end enables one to distinctly see the edges of the interference region in the plot.

The plot of the reactive energy shows four non-zero density regions of equal shape and maximum of 0.5. Hence, in the regions of destructive interference of the fields the densities of energy and reactive energy have equal maxima, where—in accordance with Eq. (A4)—the energy flow velocity vanishes. These equalities do not depend on the angle θ . On the contrary, the ratio of the maxima in the two plots depends on θ (or on $\beta = v/c = 1/\cos \theta$) according to the following expression

$$\frac{\max(w)}{\max(R)} = \frac{1 + \cos^2 \theta}{1 - \cos^2 \theta} = \frac{\beta^2 + 1}{\beta^2 - 1}, \quad (6)$$

which gives the value 7 for $\theta = 30^\circ$. The observations listed above and Eq. (6) follow from the behavior of the field vectors \mathbf{E} and \mathbf{B} in the interference region and, in particular, from their orthogonality due to which the second term $I_2 = \mathbf{E} \cdot \mathbf{B}$ in Eq. (A2) vanishes. Consequently, the reactive energy density becomes $R = (\varepsilon_0/2)|(\mathbf{E}^2 - c^2\mathbf{B}^2)|$, while the energy density is the sum of the two terms, see Eq. (4). Although this holds for all subsequent 3D TM electromagnetic localized waves, Eq. (6) is not valid because the maxima values of the energy and energy densities may occur at different locations.

We see that, indeed, the reactive energy appears only where there is an interference of the component plane waves. We conclude also from Fig. 2 that the spatial density distribution of the reactive energy moves superluminally in the z direction and—in contradistinction to that of the energy distribution—has no X-like “wings”, i.e., is completely localized in both directions. Moreover, as will be discussed in section 5, it is Lorentz-invariant, i.e., the density is the same in all inertial reference frames (see Appendix A).

III. REACTIVE ENERGY IN SUPERLUMINAL X WAVES

In this and the next section we will consider three-dimensional (3D) waves. We start with a simple axisym-

metric scalar wave pulse known under the name "fundamental X-wave", first derived in [33, 34] and since then studied by many authors. Its complex-valued expression in cylindrical coordinates (ρ, φ, z) , normalized to unity at its maximum, reads

$$\psi_X(\rho, z, t) = \frac{a}{\sqrt{\rho^2 + [a + i\tilde{\gamma}(z - vt)]^2}}. \quad (7)$$

Here, $\tilde{\gamma} \equiv 1/\sqrt{(v/c)^2 - 1}$ is the superluminal version of the Lorentz factor and v is a superluminal group velocity identical to the speed of propagation of the whole pulse. The positive free parameter a determines the width of the unipolar Lorentzian-like temporal profile of the pulse modulus on the z axis. In a meridional plane ($x = \pm\rho, z$) the double-conical spatial profile of the field energy density looks like the letter "X" and the branches of "X" are inclined with respect to x axis under the angle $\theta = \arccos \beta^{-1} = \arccos c/v$.

We deal first with the real scalar wave solution $u_X(\rho, z, t) = \text{Re} \psi_X(\rho, z, t)$ of Eq. (7) in order to ensure Lorentz-invariance of the reactive energy density (see Appendix B) which is essential for its physical interpretation and comparison with the following cases of vector-valued EM fields. Fig. 3 juxtaposes the densities w and R calculated from Eq. (B4) and (B5), respectively. These plots, as well as the rest in this Section, have been obtained by introducing the dimensionless variables $(X, Y, Z) = (x, y, z)/a$ and $T = ct/a$, using a normalized speed $c = 1$, and choosing $v/c = 1.1$. Since energy densities of 3D waves—in contradistinction to the 2D case—decrease with distance from the propagation axis z , for better display of weaker features all the following figures show colored density and surface plots.

In the given case, since the plane wave constituents of the pulse interfere, in principle, everywhere, the reactive energy is distributed over a large spatial region similarly to the energy. While the reactive energy density is generally by one order of magnitude less than that of the energy, in the central cross-sectional plane it is not so and there we see a sharp double-conical surface of zero reactive energy. Between the conical surfaces R_{\pm} —the square of the four-gradient—becomes negative, see Eq. (B6) in Appendix B.

Vector-valued X waves have been studied extensively [35–37], but we calculated here a TM version of the zeroth-order X wave. For comparison, Fig. 4 shows the distribution of the energy and reactive energy densities of such a localized wave. Since obtaining EM field vectors involves taking additional spatial and temporal derivatives (see Appendix C), the region of destructive interference is now around the apex of the cones and, consequently, the region where most of the reactive energy is located. For this particular example, the Poynting vector and, as a consequence the energy flow velocity, vanishes on axis ($x = 0$). It follows, then, that the energy and reactive energy densities coincide in this region.

Another physical interpretation can be given based on the expression of the reactive energy density given in

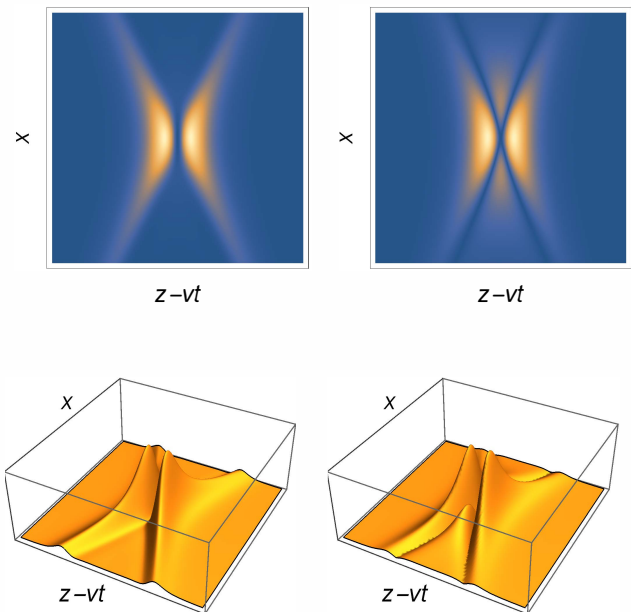


FIG. 3. Density and surface plots of the energy density (left) from Eq. (B4) and reactive energy density (right) from Eq. (B5) for the real part of the zero-order scalar X wave for a normalized speed $c = 1$ and $v/c = 1.1$. Axes $z - vt$ and x have the same range $(2a)[-1, 1]$. The ratio of the maximum values of the energy and reactive energy densities is $\max(w)/\max(R) = 10.5$ in accordance with Eq. (6).

Eq. (A4) in terms of the energy flow velocity. Away from the pulse center, the spatiotemporal distribution of the modulus of the energy flow velocity is identical to that of the energy density. In the neighborhood of the pulse center, however, the energy flow velocity is zero, but not the energy density. This is the reason for the concentration of the reactive energy density around the pulse center.

For the first-order TM field, derived from an azimuthally asymmetric scalar potential given by $\psi_X^{as}(\rho, z, \varphi, t) = (1/a)\psi_X(\rho, z, t)^3 \rho \exp(i\varphi)$, the spatiotemporal distributions of the energy density and reactive energy density are concentrated around the pulse center, albeit with different amplitudes, in accordance with Eq. (6) resulting in the ratio $\max(w)/\max(R) = 10.5238$ for the energy and reactive energy densities depicted in Fig. 5 for $\varphi = 0$.

IV. REACTIVE ENERGY IN SUBLUMINAL WAVES

The best known subluminal non-diffracting wave—the MacKinnon pulse [38] is a spherically symmetric monochromatic standing wave seen from another inertial reference frame, i.e., it is obtained by applying a Lorentz transformation with subluminal β to the z -coordinate

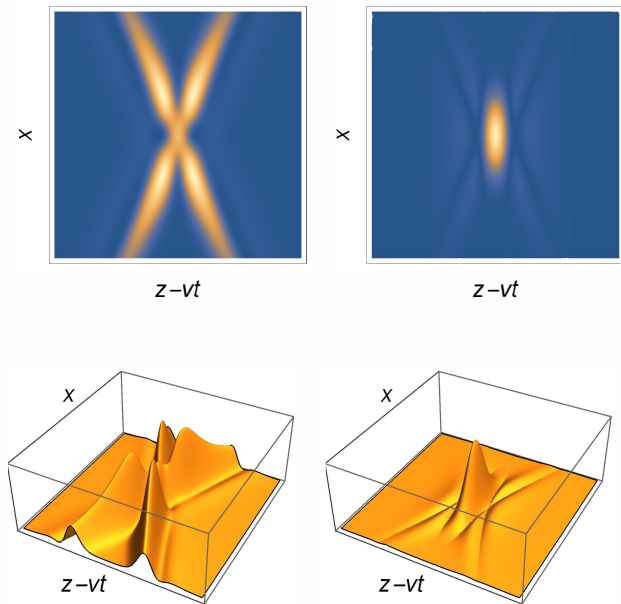


FIG. 4. Density and surface plots of the energy density (left) and reactive energy density (right) for a TM zero-order vector-valued X wave for a normalized speed $c = 1$ and $v/c = 1.1$. Axes $z - vt$ and x have the same range $(2a) [-1, 1]$ and $\max(w)/\max(R) = 1.48$.

and time [5, 7]. Its real part reads

$$\text{Re}[\psi_{MK}(\rho, z, t)] = \frac{\sin kr_t}{kr_t} \cos[k\beta\gamma(z - \tilde{v}t)], \quad (8)$$

$$r_t \equiv \sqrt{\rho^2 + \gamma^2(z - vt)^2}.$$

Eq. (8) indicates that the envelope moves rigidly along the z axis with the subluminal velocity $v = \beta c$, whereas the modulation superluminally with $\tilde{v} \equiv \beta^{-1}c = c^2/v$. In addition, the *sinc*-function-like amplitude distribution is no longer spherically symmetric as it is in the wave's rest frame, but has been compressed in the axial direction due to the Fitzgerald-Lorentz contraction. Here, we restrict the discussion to the scalar-valued wave. The energy and reactive energy density plots are shown in Fig. 6. In the rest frame of the pulse, i.e., if $v = 0$, both plots would show spherical symmetry. The plots in Fig. 6 have been obtained by introducing the dimensionless variables $(X, Y, Z) = k(x, y, z)$ and $T = kct$, using the normalized speed $c = 1$, and choosing $v/c = 0.9$ and $vt = 0$.

Due to the sinusoidal modulation of the MacKinnon pulse, the same results as those depicted in Fig. 6 would appear periodically at $t = 2\pi n\gamma/(kc)$, $n = 1, 2, 3, \dots$. It is interesting to contrast this behavior to that of the standing spherical wave $\sin kr \sin kct / r$. In this case, the energy and reactive energy densities coincide, i.e., all energy is reactive, for $t = \pi n/(kc)$, $n = 0, 1, 2, \dots$. It should be mentioned that whereas the reactive energy appears predominantly in standing waves, it is inherent also to the monochromatic expanding spherical wave $\sin[k(r - ct)]/r$ until it becomes a plane wave at infinity.

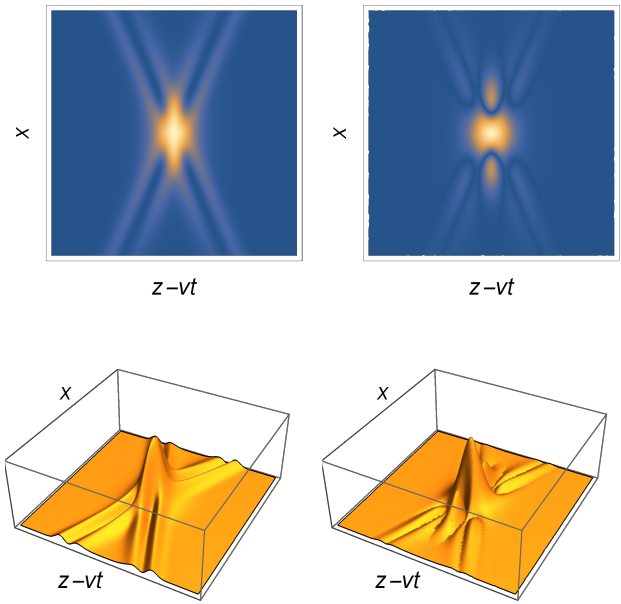


FIG. 5. Density and surface plots of the energy density (left) and reactive energy density (right) for a TM first-order (asymmetric) vector-valued X wave for a normalized speed $c = 1$, $v/c = 1.1$ and $\varphi = 0$. Axes $z - vt$ and x have the same range $(2a) [-1, 1]$ and $\max(w)/\max(R) = 10.5$.

The last spatiotemporally localized field we studied was in a sense a most physical one—the *finite* energy subluminal splash mode [39–41]. It arises from the elementary azimuthally symmetric solution $(\rho^2 + z^2 - c^2t^2)^{-1}$ of the scalar wave equation by first resorting to the complexification $t \rightarrow t + ia$ and subsequently undertaking a subluminal Lorentz transformation involving the coordinates z and t . The spatiotemporal distributions of the energy density and the reactive energy density corresponding to the vector-valued TM fields in this case (shown in Fig. 7) bare some similarity to those for the TM fields of the zero-order X Wave. As in the latter case, the reactive energy density is concentrated around the pulse center. On axis ($x = 0$) the Poynting vector vanishes; therefore, the energy and reactive energy densities coincide in this region. The same similarity exists between the scalar-valued zero-order real part of the X wave, discussed earlier, and the scalar-valued real part of the finite-energy subluminal splash mode.

V. DISCUSSION

The main and expected conclusion from all plots is that the reactive energy density appears in the regions where interference between plane wave constituents with different propagation directions takes place. Alternatively, the reactive energy is minimum when the modulus of the energy flow velocity is close to the speed of light in vacuum, and approaches the value of the energy density in

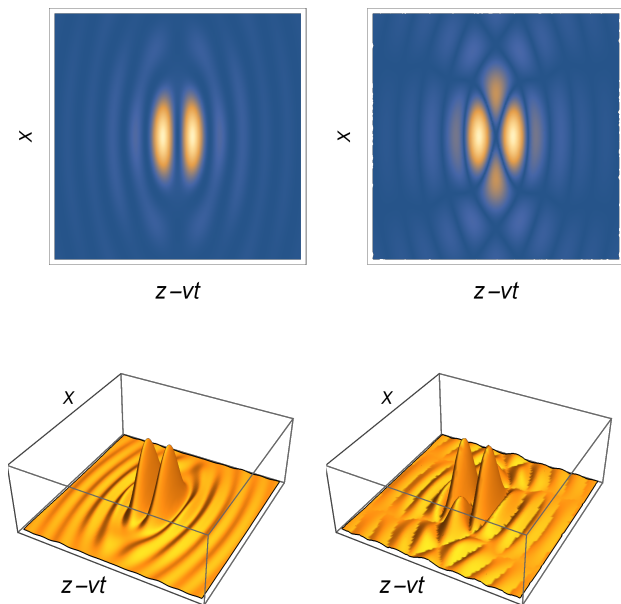


FIG. 6. Density and surface plots of the energy density (left) and reactive energy density (right) for the real part of the scalar MacKinnon subluminal wave packet for normalized speed $c = 1$ and $v/c = 0.9$. Axes x and $z - vt$ have the same range $(5/k)[-1, 1]$; $\max(w)/\max(R) = 15.6$ at $t = 0$.

the limit as the energy flow velocity approaches zero. In a sense, the reactive energy appears at the expense of decrease of the energy density w in the interference regions. This may serve as an explanation of the paradoxical circumstance that the energy flow velocity is not only smaller than the superluminal pulse propagation velocity but also smaller than c , as was shown in Ref. [19].

As mentioned in Sect. II, Fig. 2 can be equivalently considered as showing temporal dependence of the energy densities on a plane with fixed value of z , and, due to the symmetry of the plots, the time axis may be thought of as directed also from the left to the right. For an observer in a reference frame moving along the z axis with subluminal velocity c^2/v , all 3D X-type propagation-invariant waves are seen as first collapsing and then expanding cylindrical pulses with z -independent energy distributions [5, 7]. In the given 2D case, such an observer sees two plane wave pulses counterpropagating (under angle $2\theta = \pi$ with respect to each other) along the x axis, and for the observer Fig. 2 shows temporal evolution of distributions of both energy densities, which is independent of the coordinate z . Hence, for the moving observer Fig. 2 demonstrates explicitly that the reactive energy exists nowhere in the space initially, it is *created* when the pulses collide, and it disappears after that. Likewise, in the laboratory frame the superluminal movement of the reactive energy may be interpreted rather as its continuous creation and disappearance at successive locations. This may serve as an additional argument for the solution of the paradoxical feature of the energy flow velocity.

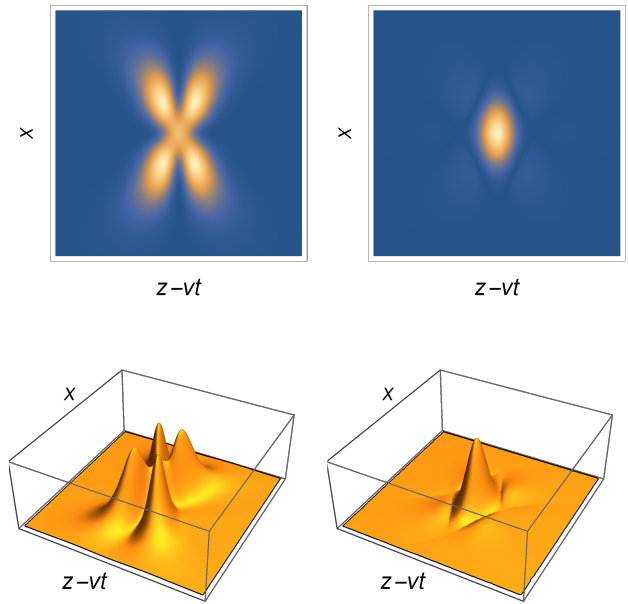


FIG. 7. Density and surface plots of the energy density (left) and reactive energy density (right) for a TM finite-energy subluminal vector-valued splash mode for normalized speed $c = 1$, $v/c = 0.9$ and $t = 0$. Axes ranges $z - vt \in (4a/5)[-1, 1]$ and $x \in (2a)[-1, 1]$; $\max(w)/\max(R) = 1.43$.

It should be noted that according to Eq. (A3) the Lorentz invariant I_1 is negative if the magnitude of $c\mathbf{B}$ exceeds that of the electric field \mathbf{E} . Thus, although by definition of the reactive energy density through the square root it is always non-negative, in the cases when $\mathbf{E} \cdot \mathbf{B} = 0$ we may consider an alternative definition of the density $R_{\pm} = \epsilon_0 (\mathbf{E}^2 - c^2 \mathbf{B}^2) / 2$. For example, within the two rhombus-like regions on the horizontal axis on the right-hand plot of Fig. 2, $R_{\pm} < 0$ because the magnetic field is stronger than the electric field there. If the pulse was unipolar, R_{\pm} would be positive nowhere. The X-like cross of dark lines in the plot that separates the four regions indicates the points where $R = |R_{\pm}| = 0$, i.e., R_{\pm} changes its sign. Similar zero lines are seen in all subsequent plots of R . In the case of scalar-valued fields, as seen from Eq. (B6), R_{\pm} becomes negative if the magnitude of the spatial gradient exceeds the absolute value of the time derivative of the field. Understandably, the quantity R_{\pm}/c^2 cannot be interpreted as a mass density. This fact, to a certain degree, undermines the known interpretation [24, 27] of R/c^2 as the rest mass density of the field.

In the case of infinite-energy non-diffracting fields, it does not make much sense to ask what is the total reactive energy. However, all such fields become finite-energy ones in reality due to the finite apertures of the devices generating them. A finite aperture ensures a finite depth and a finite duration of diffraction-free propagation. Outside of the region of diffraction-free propagation the pulse develops into a spherical wave with velocity c which be-

comes a plane wave at infinity. Thus, with reference to Eq. (A4), we can conclude that the spatio-temporal region where the reactive energy is not vanishingly small, is always finite for real pulses. Despite the fact that the reactive energy density is Lorentz-invariant, the total reactive energy $\int R dx dy dz$ is not [28]. However, following the example of the invariant action as four-integral of the Lagrangian density, we can construct the quantity $\int R_{\pm} dx dy dz dt$ which is Lorentz-invariant and might be called 'reactive action'. It is interesting to note that if $\mathbf{E} \cdot \mathbf{B} = \mathbf{0}$, the reactive energy density R_{\pm} coincides with the Lagrangian density of the field and, hence, the 'reactive action' is equal to the action. On the other hand, it is known that if one *first* integrates over all space separately the energy and momentum density of the pulse, and then takes the difference of their squares, i.e., the difference of squares of total energy W and total momentum multiplied by c , *viz.*

$$\left(\int w dx dy dz \right)^2 - \left(\frac{1}{c} \int \mathbf{S} dx dy dz \right)^2 = W^2 - (c\mathbf{P})^2, \quad (9)$$

one gets a quantity which is the same in all inertial reference frames (see, e.g., Ref. [42]). The quantity given in Eq. (9) is the square of the total reactive energy and its division by c^4 can be considered as the square of the invariant rest mass of the pulse [24, 27, 28]. The reasons why the integral $(\int R dx dy dz)^2$ calculated using Eq. (5) does not give the same invariant quantity are obvious. Mathematically, two operations—integration and taking the difference of squares—are carried out in different order in either case. Physically, Eq. (9) characterises reactive energy globally, while Eq. (5)—locally.

Considering, finally, the complex time-dependent Poynting vector as $\mathbf{S}(\mathbf{r}, t) = \mathbf{E}(\mathbf{r}, t) \times \mathbf{H}^*(\mathbf{r}, t)$, we obtain the "conservation" law

$$\nabla \cdot \mathbf{S} + \varepsilon_0 \left(\mathbf{E} \cdot \frac{\partial}{\partial t} \mathbf{E}^* + c^2 \mathbf{B} \cdot \frac{\partial}{\partial t} \mathbf{B}^* \right) = 0. \quad (10)$$

Writing the complex Poynting vector explicitly in terms of its real and imaginary parts, *viz.*, $\mathbf{S} = \mathbf{S}_r + i\mathbf{S}_i$, we obtain

$$\nabla \cdot \mathbf{S}_r + \frac{\partial}{\partial t} w_r; \quad w_r = \frac{\varepsilon_0}{2} (\mathbf{E} \cdot \mathbf{E}^* + c^2 \mathbf{B} \cdot \mathbf{B}^*), \quad (11)$$

and for the imaginary part of the Poynting vector

$$\nabla \cdot \mathbf{S}_i + \varepsilon_0 \operatorname{Im} \left\{ \mathbf{E} \cdot \frac{\partial}{\partial t} \mathbf{E}^* + c^2 \mathbf{B} \cdot \frac{\partial}{\partial t} \mathbf{B}^* \right\} = 0. \quad (12)$$

For time-harmonic fields, Eq. (12) would result in the conventional reactive energy density.

VI. CONCLUSIONS

The notion of "reactive energy" has been of fundamental importance in assessing the efficiency of monochromatic radiating structures by evaluating the stored (non-propagating) energy in the near field [45]. With the

widespread applications of wideband pulsed signals, attempts have been made recently to expand the concept of reactive energy to the time domain. Different approaches have been followed along this direction. Recently Mikki, Sarkar and Antar [46], for example, have introduced the "localized energy density" defined as the difference of the electromagnetic energy density and the modulus of the Poynting vector divided by c in free space.

In this article, we have adopted the definition of the reactive energy density $R = \sqrt{w^2 - \mathbf{S}^2/c^2}$, see Eqs. (3)-(5), introduced by Kaiser [24] by analogy to the rest energy $E_0 = \sqrt{E^2 - c^2 \mathbf{p}^2}$ of a relativistic point particle having total energy E and momentum \mathbf{p} . The ratio R/c^2 is defined as the rest mass density of the fields [24, 27]. The reactive energy density is Lorentz invariant and for fields where $\mathbf{E} \cdot \mathbf{B} = \mathbf{0}$, the reactive energy density coincides with the Lagrangian density. Proofs of the Lorentz invariance are given in Appendices A and B for vector-valued and scalar-valued electromagnetic fields, respectively.

The definition of the time-dependent reactive energy density R in Eq. (5) has been used in this article mostly as a measure of "interference" in order to explain and illustrate the difference between the energy flow velocity and the group velocity in structured light pulses. Specific numerical results have been presented for basic types of scalar-valued and vector-valued superluminal and subluminal spatiotemporally localized electromagnetic waves in vacuum. The main conclusion has been that the reactive energy density is larger in regions of strong interference of the constituent plane wave components of the structured light field pulses. Alternatively, the reactive energy is minimum when the modulus of the energy flow velocity is close to the speed of light in vacuum and approaches the value of the energy density in the limit as the energy flow velocity approaches zero.

Appendix A: PROOF OF LORENTZ INVARIANCE OF REACTIVE ENERGY DENSITY FOR EM FIELDS

Reactive energy and its quotient by c^2 —reactive mass density—are the same in different inertial reference frames [24, 27]. Here we give another proof of this remarkable property and relate these quantities to energy flow and group velocities.

Let us compose the complex-valued Riemann-Silberstein vector from the real-valued electric and magnetic fields satisfying the homogeneous Maxwell equations in free space

$$\mathbf{F} = \sqrt{\frac{\varepsilon_0}{2}} (\mathbf{E} + ic\mathbf{B}). \quad (A1)$$

Certain important physical quantities associated with the real fields $\mathbf{E}(\mathbf{r}, t)$ and $\mathbf{B}(\mathbf{r}, t)$ can be expressed conveniently in terms of $\mathbf{F}(\mathbf{r}, t)$. Specifically, the Poynting vector \mathbf{S} and the electromagnetic field energy density w —see

also Eqs. (3) and (4)— can be written as

$$\begin{aligned}\mathbf{S} &= -ic\mathbf{F}^* \times \mathbf{F} , \\ w &= \mathbf{F}^* \cdot \mathbf{F} ,\end{aligned}\quad (\text{A2})$$

where the asterisk denotes complex conjugation. The reactive energy density given in Eq. (5) can be written in terms of the Riemann-Silberstein vector and the fields as

$$\begin{aligned}R &= |\mathbf{F} \cdot \mathbf{F}| = \sqrt{\frac{\varepsilon_0^2}{4} I_1^2 + \varepsilon_0^2 c^2 I_2^2} ; \\ I_1 &= \mathbf{E}^2 - c^2 \mathbf{B}^2, \quad I_2 = \mathbf{E} \cdot \mathbf{B} .\end{aligned}\quad (\text{A3})$$

Both I_1 and I_2 are well-known Lorentz invariants. As consequence, the reactive energy density R is Lorentz-invariant. It can also be expressed as

$$R = w \sqrt{1 - \frac{|\mathbf{v}_e|^2}{c^2}} , \quad (\text{A4})$$

in terms of the electromagnetic energy density and the local energy flow velocity \mathbf{v}_e . In locations where \mathbf{v}_e is parallel to z axis and Eq. (1) holds, we obtain

$$R = w \left| \frac{1 - \beta^2}{1 + \beta^2} \right| , \quad (\text{A5})$$

where $\beta = v_g/c$ is the normalized group velocity. It follows, then, that the reactive energy density is maximum (equal to w) when $\mathbf{v}_e = 0$ (or $v_g = 0$, i.e., the pulse is not moving in the z direction) and equals zero when $\mathbf{v}_e = c$ (or $v_g = c$). The latter is the case for null electromagnetic waves, which are also characterized by the fact that both I_1 and I_2 equal zero.

Appendix B: PROOF OF LORENTZ INVARIANCE OF REACTIVE ENERGY DENSITY FOR SCALAR FIELDS

Optical fields, especially paraxial ones, can be in good approximation described by a single scalar function $\psi(x, y, z, t)$. In this case, the Poynting vector \mathbf{S} and energy density w are given by the expressions [43, 44].

$$\frac{\mathbf{S}}{\alpha c} = -(\partial_{ct}\psi^*)(\nabla\psi) - (\partial_{ct}\psi)(\nabla\psi^*) , \quad (\text{B1a})$$

$$\frac{w}{\alpha} = (\partial_{ct}\psi)(\partial_{ct}\psi^*) + (\nabla\psi) \cdot (\nabla\psi^*) , \quad (\text{B1b})$$

where ∂_{ct} denotes the derivative with respect to ct , and α is a positive constant whose value depends on the choice of units. The expressions have been written so that the right-hand sides are of the same dimension.

Using Eqs. (5), (B1a), and (B1b), we obtain for square of the reactive energy density the following expression:

$$\begin{aligned}\frac{R^2}{\alpha^2} &= \left[(\partial_{ct}\psi)^2 - (\partial_x\psi)^2 - (\partial_y\psi)^2 - (\partial_z\psi)^2 \right] \\ &\times \left[(\partial_{ct}\psi^*)^2 - (\partial_x\psi^*)^2 - (\partial_y\psi^*)^2 - (\partial_z\psi^*)^2 \right] \\ &- [(\partial_x\psi^*)(\partial_y\psi) - (\partial_y\psi^*)(\partial_x\psi)]^2 \\ &- [(\partial_x\psi^*)(\partial_z\psi) - (\partial_z\psi^*)(\partial_x\psi)]^2 \\ &- [(\partial_z\psi^*)(\partial_y\psi) - (\partial_y\psi^*)(\partial_z\psi)]^2 .\end{aligned}\quad (\text{B2})$$

The first term on the right-hand side is Lorentz invariant, but not the remaining three terms. Therefore, the reactive energy density of the complex-valued scalar field ψ is not Lorentz invariant. It should be noted, however, that for a real field $u(x, y, z, t)$ which can be either the real or the imaginary part of $\psi(x, y, z, t)$, the Poynting vector and energy density are defined as

$$\frac{\mathbf{S}}{\alpha c} = -2(\partial_{ct}u)(\nabla u) , \quad (\text{B3})$$

$$\frac{w}{\alpha} = (\partial_{ct}u)^2 + (\nabla u) \cdot (\nabla u) . \quad (\text{B4})$$

In this case, the reactive energy density R is Lorentz invariant because with taking $\alpha = 1$, Eq. (B2) reduces to

$$R = \left| (\partial_{ct}u)^2 - (\partial_xu)^2 - (\partial_yu)^2 - (\partial_zu)^2 \right| . \quad (\text{B5})$$

It is interesting to note that in the case of scalar fields, as it follows from Eq. (B2), one can define a quantity

$$R_{\pm} = (\partial_{ct}u)^2 - (\partial_xu)^2 - (\partial_yu)^2 - (\partial_zu)^2 , \quad (\text{B6})$$

which is also Lorentz invariant with dimension of energy, but can acquire negative values in regions where the square of the four-gradient is negative. Let us add that although the quantity $|\psi(x, y, z, t)|^2$ is often used in the role of the energy density, it is correct only for paraxial scalar fields.

To our best knowledge, the results of this Appendix have been obtained for the first time.

Appendix C: TRANSVERSE MAGNETIC (TM) VECTOR FIELDS

A real-valued electric vector Hertz potential $\mathbf{\Pi}_e(\mathbf{r}, t)$ is defined as follows:

$$\mathbf{\Pi}_e(\mathbf{r}, t) = \mathbf{e}_z \text{Re} \{ \psi(\mathbf{r}, t) \} .$$

Here, \mathbf{e}_z is a unit vector along the z direction and $\psi(\mathbf{r}, t)$ is a subluminal or superluminal localized solution to the scalar wave equation in free space. The corresponding real TM electromagnetic fields are given by

$$\mathbf{E}(\mathbf{r}, t) = \nabla \nabla \cdot \mathbf{\Pi}_e(\mathbf{r}, t) - \frac{1}{c^2} \frac{\partial^2}{\partial t^2} \mathbf{\Pi}_e(\mathbf{r}, t) ,$$

$$\mathbf{H}(\mathbf{r}, t) = \varepsilon_0 \nabla \times \frac{\partial}{\partial t} \mathbf{\Pi}_e(\mathbf{r}, t) .$$

With $\mathbf{B}(\mathbf{r}, t) = \mu_0 \mathbf{H}(\mathbf{r}, t)$ in vacuum, the energy and reactive energy densities can be computed using Eqs. (A1)-(A3). Due to the invariance of the energy flux and en-

ergy density with respect to the duality transformation $\mathbf{E} \rightarrow c\mathbf{B}$, $\mathbf{B} \rightarrow -\mathbf{E}/c$ the results obtained in this paper for TM pulses apply also for TE pulses.

-
- [1] P. Saari, Reexamination of group velocities of structured light pulses, *Phys. Rev. A*, **97**, 063824 (2018).
- [2] *Localized Waves*, edited by H. E. Hernandez-Figueroa, M. Zamboni-Rached, and E. Recami (J. Wiley, New York, 2007).
- [3] *Non-Diffracting Waves*, edited by H. E. Hernandez-Figueroa, E. Recami, and M. Zamboni-Rached (J. Wiley, New York, 2013).
- [4] R. Donnelly and R. Ziolkowski, Designing localized waves, *Proc. R. Soc. Lond. A* **440**, 541 (1993).
- [5] I. Besieris, M. Abdel-Rahman, A. Shaarawi, and A. Chatzipetros, Two fundamental representations of localized pulse solutions to the scalar wave equation, *Progr. in Electrom. Res.* **19**, 1 (1998).
- [6] J. Salo, J. Fagerholm, A. T. Friberg, and M. M. Salomaa, Unified description of nondiffracting X and Y waves, *Phys. Rev. E*, **62**, 4261 (2000).
- [7] P. Saari and K. Reivelt, Generation and classification of localized waves by Lorentz transformations in Fourier space, *Phys. Rev. E* **69**, 036612 (2004).
- [8] A. P. Kiselev, Localized light waves: paraxial and exact solutions of the wave equation (a Review), *Optics and Spectroscopy* **102**, 603 (2007).
- [9] M. Yessenov, B. Bhaduri, H. E. Kondakci, and A. F. Abouraddy, Classification of propagation-invariant space-time wave packets in free space: theory and experiments, *Phys. Rev. A* **99**, 023856 (2019).
- [10] P. Saari and K. Reivelt, Evidence of X-shaped propagation-invariant localized light waves, *Phys. Rev. Lett.* **79**, 4135 (1997).
- [11] J. Durnin, J. J. Miceli, and J. H. Eberly, Diffraction-free beams, *Phys. Rev. Lett.* **58**, 1499 (1987).
- [12] I. Alexeev, K. Y. Kim, and H. M. Milchberg, Measurement of the superluminal group velocity of an ultrashort Bessel beam pulse, *Phys. Rev. Lett.* **88**, 073901 (2002).
- [13] R. Grunwald, V. Kebbel, U. Griebner, U. Neumann, A. Kummrow, M. Rini, E. T. J. Nibbering, M. Piché, G. Rousseau, and M. Fortin, Generation and characterization of spatially and temporally localized few-cycle optical wave packets, *Phys. Rev. A* **67**, 063820 (2003).
- [14] P. Bowlan, H. Valtna-Lukner, M. Löhmus, P. Piskarv, P. Saari, and R. Trebino, Measurement of the spatiotemporal field of ultrashort Bessel-X pulses,” *Opt. Lett.*, **34**, 2276 (2009).
- [15] P. Bowlan, H. Valtna-Lukner, M. Löhmus, P. Piskarv, P. Saari, and R. Trebino, Measurement of the spatiotemporal electric field of ultrashort superluminal Bessel-X pulses,” *Optics and Photonics News* **20**, 42 (2009).
- [16] H. E. Kondakci and A. F. Abouraddy, Diffraction-free space-time light sheets, *Nature Photonics* **11**, 733 (2017).
- [17] B. Bhaduri, M. Yessenov, and A. F. Abouraddy, Space-time wave packets that travel in optical materials at the speed of light in vacuum, *Optica* **6**, 139 (2019).
- [18] H. E. Kondakci and A. F. Abouraddy, Optical space-time wavepackets having arbitrary group velocities in free space, *Nature Commun.* **10**, 08735-1-8 (2019).
- [19] P. Saari, O. Rebane, and I. Besieris, Energy-flow velocities of nondiffracting localized waves, *Phys. Rev. A* **100**, 013849 (2019).
- [20] J. D. Jackson, *Classical Electrodynamics*, 3rd ed. (New York: Wiley 1998).
- [21] J. Lekner, Phase and transport velocities in particle and electromagnetic beams, *J. Opt. A: Pure Appl. Opt.* **4**, 491 (2002).
- [22] I. M. Besieris and A.M. Shaarawi, Spatiotemporally localized null electromagnetic waves I. Luminial, *Progress in Electromagnetic Research (PIER)* **B 8**, 1 (2008).
- [23] I. M. Besieris and A. M. Shaarawi, Spatiotemporally localized null electromagnetic waves, in [3], p. 161.
- [24] G. Kaiser, Electromagnetic inertia, reactive energy and energy flow velocity, *J. Phys. A: Math. Theor.* **44**, 345206 (2011).
- [25] P. Saari, Localized waves in femtosecond optics, in *Ultrafast Photonics*, (Bristol and Philadelphia: IoP Publishing 2004) p. 317-340.
- [26] P. Saari, X-type waves in ultrafast optics, in [3] p. 109.
- [27] S. V. Vintskevich, V. G. Veselago, and M. V. Fedorov, On a possible definition of the concept of ‘mass density’ for a classical electromagnetic field in vacuum, *Laser Phys. Lett.* **12**, 096201 (2015).
- [28] M. V. Fedorov and S. V. Vintskevich, Diverging light pulses in vacuum: Lorentz-invariant mass and mean propagation speed, *Laser Phys.* **27**, 036202 (2017).
- [29] S. V. Vintskevich and D. A. Grigoriev, Structured light pulses and their Lorentz-invariant mass, *Laser Phys.* **29**, 086001 (2019).
- [30] H. E. Kondakci and A. F. Abouraddy, Self-healing of space-time light sheets, *Opt. Lett.* **43**, 30-3832 (2018).
- [31] M. Yessenov, B. Bhaduri, L. Mach, D. Mardani, H. E. Kondakci, M. A. Alonso, G. A. Atia, and A. F. Abouraddy, “What is the maximum differential group delay achievable by a space-time wave packet in free space?” *Opt. Express*, **27**, 12443 (2019).
- [32] B. Bhaduri, M. Yessenov, and A. F. Abouraddy, Dynamical refraction of optical space-time wave packets, *Opt. Lett.* **XX**, XX (in press) (2019).
- [33] J. Y. Lu, and J. F. Greenleaf, Nondiffracting X waves—exact solutions to free space scalar wave equations and their aperture realizations, *IEEE Trans. Ultrason. Ferroelec. Freq. Contr.* **39**, 19 (1992).
- [34] R. W. Ziolkowski, I. M. Besieris, and A. M. Shaarawi, Aperture realizations of the exact solutions to homogeneous-wave equations, *J. Opt. Soc. Am. A* **10**, 75 (1993).
- [35] E. Recami, On localized “X-shaped” superluminal solutions to Maxwell equations, *Physica A* **252**, 586 (1998).
- [36] D. Mugnai and I. Mochi, Superluminal X-wave propagation: energy localization and velocity, *Phys. Rev. E* **73**, 016606 (2005).
- [37] M. A. Salem and H. Bağcı, Energy flow characteristics of vector X-waves, *Opt. Express*, **19**, 8526 (2011).
- [38] L. A. Mackinnon, A nondispersive de Broglie wave

- packet, *Found. Phys.* **8**, 157 (1978).
- [39] R. Ziolkowski, Exact solutions of the wave equation with complex source locations, *J. Math. Phys.* **26**, 861 (1985).
- [40] R. Ziolkowski, Localized transmission of electromagnetic energy, *Phys. Rev. A* **39**, 2005 (1989).
- [41] I. M. Besieris, A. Shaarawi, and R. Ziolkowski, A bidirectional traveling plane wave representation of exact solutions of the scalar wave equation," *J. Math. Phys.* **30**, 1254 (1989).
- [42] J. Lekner, *Theory of electromagnetic pulses*, (San Rafael, Calif. Morgan & Claypool 2018).
- [43] H. S. Green and E. Wolf, A Scalar representation of electromagnetic fields, *Proc. Phys. Soc. A* **66**, 1129 (1953).
- [44] L. Mandel and E. Wolf, *Optical Coherence and Quantum Optics* (Cambridge University Press, 1995), p. 288.
- [45] M. Capek, L. Jelinek, and G. A. E. Vandenbosch, Stored electromagnetic energy and quality factor of radiating structures, *Proc. Roy. Soc. London A* **472**, 1 (2016).
- [46] S. Mikki, D. Sarkar, and Y. M. M. Antar, On localized antenna energy in electromagnetic radiation, *Progr. Electromagn. Research (PIER) M* **79**, 1 (2019).